Research Square

Preprints are preliminary reports that have not undergone peer review.
They should not be considered conclusive, used to inform clinical practice,
or referenced by the media as validated information.

Estimation of Heat Transfer Characteristics of Inclined Cylinders with Different Fins Using Machine Learning

ibrahim ŞAFAK

ibrahimsafak@kayseri.edu.tr

Kayseri Üniversitesi

Aslı DURMUŞOĞLU

Hakkari University

Sibel GÜNEŞ

Erciyes University

Research Article

Keywords: Natural Convection, Annular Fins, Thermal Performance Estimation, Gaussian Process Regression

Posted Date: November 18th, 2026

DOI: https://doi.org/10.21203/rs.3.rs-11491188/v1

License: This work is licensed under a Creative Commons Attribution 4.0 International License.
Read Full License

Additional Declarations: No competing interests reported.

Estimation of Heat Transfer Characteristics of Inclined Cylinders with Different Fins Using Machine Learning

İbrahim ŞAFAK[1*], Aslı DURMUŞOĞLU[2†] and Sibel GÜNEŞ[3]

[1*]Machine and Metal Technologies, Vocational School of Technical Sciences, Kayseri University, 38280, Kayseri, TÜRKİYE.
[2]Mechanical Engineering, Engineering Faculty, 30100, Hakkari, TÜRKİYE.
[3]Mechanical Engineering, Engineering Faculty, 380330, Kayseri, TÜRKİYE.

*Corresponding author(s). E-mail(s): ibrahimsafak@kayseri.edu.tr;
Contributing authors: aslidurmusoglu@hakkari.edu.tr;
sgumus@erciyes.edu.tr;
†These authors contributed equally to this work.

Abstract

Natural convection from annular-finned cylinders depends on coupled effects of fin arrangement, inclination, heat input, and material properties that are difficult to capture using conventional correlations. This study presents a data-driven framework for estimating the Nusselt number (Nu) and thermal resistance ($\boldsymbol{R}_{\mathrm{th}}$) of cylinders equipped with homogeneous aluminum and functionally graded Al–Cu fins. The dataset contains 360 experimental observations covering five fin configurations, inclination angles from $\mathbf{0}^{\circ}$ to $\mathbf{75}^{\circ}$, and heat-input levels from 25 to 150 W. Gaussian process regression (GPR), a Bayesian regularized artificial neural network (BRANN), and XGBoost were evaluated. Generalization was assessed using leave-one-power-level-out, leave-one-angle-out, and leave-one-fin-configuration-out validation. Accumulated local effects analysis was used to interpret GPR, and symbolic regression provided explicit correlations for both outputs. GPR achieved the highest accuracy. Under the primary leave-one-angle-out validation, its $\boldsymbol{R}^{\mathbf{2}}$ values ranged from 0.989 to 0.992 for Nu and from 0.988 to 0.991 for $\boldsymbol{R}_{\mathrm{th}}$, with corresponding MAPE ranges of 1.458–1.518% and 3.273–4.375%. The 95% prediction intervals achieved empirical coverage rates

of 92.8–95.6%, with the widest intervals occurring when an entire fin configuration was excluded. The symbolic correlations produced $\boldsymbol{R^2}$ values of 0.955–0.975. Increasing the Rayleigh number enhanced Nu, whereas increasing inclination weakened convection and raised $\boldsymbol{R}_{\mathrm{th}}$. An intermediate fin-spacing ratio maximized the normalized convective response, while denser arrangements reduced thermal resistance. Functionally graded Al–Cu fins generally increased Nu and decreased $\boldsymbol{R}_{\mathrm{th}}$ relative to aluminum fins. The framework combines accurate estimation, calibrated uncertainty, physical interpretation, and compact engineering correlations for inclined annular-finned cylinders.

Keywords: Natural Convection; Annular Fins; Thermal Performance Estimation; Gaussian Process Regression

1 Introduction

Natural convection is widely used in thermal systems where quiet operation, low maintenance requirements, and the absence of external power consumption are important design considerations. Nevertheless, the relatively low heat transfer coefficient associated with natural convection often limits its effectiveness, particularly in compact devices exposed to moderate or high thermal loads. Extended surfaces offer a practical means of overcoming this limitation by increasing the effective heat transfer area without introducing additional energy consumption. Among the available configurations, annular fins mounted on cylindrical surfaces are frequently encountered in heat exchangers, electronic cooling equipment, storage units, process systems, and other passive thermal management applications. Their performance, however, is governed not only by the added surface area but also by the interaction among fin spacing, fin number, material properties, surface temperature, and cylinder orientation.

Recent studies have examined annular fins under a broad range of thermal and geometrical conditions. Numerical investigations have addressed the effects of radiation, natural convection, internal heat generation, nanomaterial properties, and particle morphology on annular-fin performance [1, 2]. Related studies have extended this framework to radiated surfaces, nucleate boiling conditions, and advanced nanomaterials [3]. Annular fins have also been investigated in latent heat storage systems, where fin dimensions and arrangement influence the melting process and overall charging response [4, 5]. Although these studies demonstrate the versatility of annular fins, many of them concern idealized numerical domains, phase-change systems, or nanofluids. Their findings therefore cannot be transferred directly to an experimentally tested, air-cooled inclined cylinder equipped with homogeneous and functionally graded annular fins.

Cylinder orientation introduces an additional level of complexity because buoyancy-driven flow is sensitive to the direction of gravity relative to the heated surface. Changes in inclination can alter boundary-layer development, plume formation, air circulation between neighboring fins, and the chimney effect. Earlier work showed that artificial neural networks could represent natural convection from vertical and inclined arrays of horizontal cylinders [6]. Thermo-hydraulic behavior in

slightly inclined finned channels [7], the performance of interrupted and staggered inclined-fin arrays [8], and heat transfer from surfaces subjected to different approach angles [9] have since been investigated using experimental, numerical, and data-based approaches. More recently, Kim and Kim [10] experimentally studied curved finned cylinders at different inclination angles and developed a Nusselt number correlation incorporating the effects of inclination, fin number, and Rayleigh number. These studies confirm that orientation should not be treated as a secondary correction. It is a governing design variable whose effect depends on the entire fin configuration.

Material selection is equally important. Conventional aluminum fins provide high thermal conductivity and low weight, but a homogeneous material does not necessarily produce the most favorable temperature distribution over an extended surface. Functionally graded materials offer an alternative by allowing the thermophysical properties to vary gradually along the fin radius. This approach can redistribute thermal resistance and improve the use of the available fin area. Recent analytical and data-based investigations have reported the potential of functionally graded annular fins for thermal management [11]. However, the practical performance of such fins must ultimately be established through experiments because manufacturing conditions, contact resistance, radiation, property variation, and interactions between adjacent fins are difficult to represent completely in an idealized model.

The experimental system considered in the present study has previously been examined from several complementary perspectives. Dogmaz et al. [12] compared the thermal performance of aluminum and functionally graded annular fins mounted on a horizontal cylinder. Safak et al. [13] subsequently extended the experiments to inclined-cylinder configurations and evaluated the effects of fin material, fin number, heat input, and inclination angle on natural convection. The same experimental framework was later assessed using the Taguchi method to determine the parameter combination that maximized the Nusselt number and to quantify the contributions of the principal design variables [14]. These studies established the physical behavior of the system and demonstrated the thermal advantages associated with functionally graded fins. They did not, however, develop a predictive framework capable of estimating thermal resistance and Nusselt number throughout the experimental design space or testing whether the learned relationships remain valid for operating conditions and fin configurations excluded from model development.

Data-based prediction offers an effective way to complement conventional experimental correlations when several geometrical, material, and operating variables act simultaneously. Artificial neural networks have been applied to mixed-convection enclosures [15], inclined cylinder arrays, free convection from wavy surfaces [16], and Nusselt number prediction for inclined jet configurations [17]. Similar approaches have been used to estimate heat transfer and weight characteristics of panel radiators [18], multiple thermal parameters of helically coiled heat exchangers [19], and the experimental heat transfer rates of finned radiators [20]. Çolak et al. [21] also showed that neural networks can capture the influence of corrugation parameters on heat exchanger performance. In our previous study, a data-based model was used to estimate the thermal performance of a horizontal mantle hot-water tank equipped with obliquely

positioned obstacles [22]. Collectively, these investigations demonstrate that nonlinear predictive models can reproduce complex relationships between design parameters and thermal responses with satisfactory accuracy.

Despite these developments, two issues remain important. First, much of the available heat transfer literature relies on a single neural-network structure or evaluates models using a random division of closely related observations. When measurements obtained at the same operating level or from the same geometrical configuration are distributed across both training and test subsets, apparently high accuracy may not reflect the model's ability to predict a genuinely unseen condition. Çorumlu et al. [23] highlighted the importance of external validation when evaluating thermal parameters of heat sinks and showed that model assessment should extend beyond fitting accuracy. Second, different learning methods offer different advantages. Gaussian process regression is well suited to nonlinear regression problems involving limited data and can provide information about predictive uncertainty. Its applicability to thermal-fluid prediction has recently been demonstrated by Afzal et al. [24]. Tree-based boosting methods can capture nonlinearities and variable interactions without requiring a predetermined functional form. Noh et al. [25], for example, employed XGBoost for the prediction of a complex boiling-related thermal response. For natural convection, Biswal and Meshram [26] directly demonstrated the feasibility of predicting Nusselt number for vertical helical coils using learning-based models.

A further limitation is that prediction accuracy alone offers little physical insight. A model may reproduce the measured data accurately while providing no clear explanation of how inclination angle, fin spacing, material type, heat input, or Rayleigh number affects the predicted response. This is particularly restrictive in thermal design, where the usefulness of a predictive model depends on whether its trends remain consistent with the governing heat transfer mechanisms. Therefore, model interpretation should be incorporated into the analysis rather than treated as an optional post-processing step. In addition, conventional black-box models do not provide an explicit engineering expression that can be readily used in preliminary design calculations. A compact correlation derived from the data would make the results more transferable and allow direct comparison with conventional Nusselt number correlations.

Against this background, the present study develops a data-driven framework for predicting the natural convection characteristics of aluminum and functionally graded annular-fin arrays mounted on an inclined cylinder. The experimental database covers two fin materials, different fin numbers and normalized fin spacings, six inclination angles ranging from 0° to 75°, and multiple heat-input levels. The 90° measurements are excluded from the principal database because this orientation was not included in the original experimental design reported in the thesis-based studies. Two related prediction problems are considered. Thermal resistance is estimated using heat input, inclination angle, normalized fin spacing, and material type, whereas the Nusselt number is modeled using the Rayleigh number together with inclination angle, normalized spacing, and fin material.

Gaussian process regression is adopted as the principal predictive approach, while XGBoost and a Bayesian-regularized artificial neural network are employed as comparative models. Because GPR returns a posterior predictive distribution rather than only point estimates, 95% prediction intervals are also evaluated to determine whether the estimated uncertainty remains adequately calibrated under unseen operating and geometric conditions. Their performance is evaluated using complementary error measures rather than relying on the coefficient of determination alone. More importantly, the validation strategy is organized according to physically meaningful groups. Leave-one-heat-input, leave-one-inclination-angle, and leave-one-fin-configuration tests are used to examine whether the models can generalize to operating and geometrical conditions that are absent from the training data. Accumulated local effects analysis is then applied to identify the direction, magnitude, and nonlinear character of the influence exerted by each input variable. Finally, symbolic regression is used to derive explicit correlations for the Nusselt number and thermal resistance, thereby connecting the predictive capability of the data-driven models with equations that can be used directly in engineering calculations.

The contribution of this study is therefore not another experimental comparison of aluminum and functionally graded fins. Those physical comparisons and their Taguchi-based optimization have already been reported [12, 13]. The present work re-examines the experimental database from a predictive and generalization-oriented perspective. Its main contributions are the simultaneous estimation of thermal resistance and Nusselt number, the comparison of probabilistic, boosting, and regularized neural-network models, the use of physically grouped validation instead of a conventional random data split, the assessment of predictive uncertainty through 95% prediction intervals, the interpretation of the learned thermal relationships through accumulated local effects, and the development of explicit correlations for the Nusselt number and thermal resistance through symbolic regression. In this way, the study converts a previously characterized experimental system into a predictive engineering framework while retaining a direct connection with the underlying natural convection behavior.

2 Materials and Methods

In contrast to previous studies, this research employs a novel methodology utilizing experimental data from two distinct fin materials mounted on an aluminum cylinder at various inclination angles relative to the horizontal. Based on these measurements, new data-driven prediction models were developed to estimate heat transfer performance. The validation strategies and model evaluation criteria applied during this process are described in detail.

In the generated dataset, heating power, inclination angle, dimensionless fin spacing, and fin material defined the operating and geometric conditions. The Nusselt number and thermal resistance served as the target thermal performance parameters for estimation. The dataset was used both to characterize the measured operating points and to develop predictive models to estimate the system's thermal response under varying power, inclination, and fin-spacing conditions.

2.1 Data-Driven Estimation Framework

After constructing the experimental dataset, a unified data-driven framework was developed to estimate the thermal performance of the finned cylinder. Two complementary estimation problems were addressed. The first used the Rayleigh number, inclination angle, dimensionless fin spacing, and fin material to estimate the Nusselt number. The second used heating power, inclination angle, dimensionless fin spacing, and fin material to estimate thermal resistance. Separate models were constructed for each target variable because they represent distinct aspects of the thermal response and have different numerical scales.

The fin configuration was characterized by the dimensionless spacing ratio s/d and the fin material as a binary categorical variable. Continuous inputs were standardized using the mean and standard deviation calculated only from the respective training subset. The three regression methods, namely Gaussian Process Regression (GPR), Extreme Gradient Boosting (XGBoost), and a Bayesian-Regularized Artificial Neural Network (BRANN), were tested under identical validation conditions. GPR was the main estimator chosen because it is well-suited for relatively small experimental data sets and provides both point estimates and predictive uncertainty. XGBoost and BRANN were selected as nonlinear benchmark models. Also, an explicit correlation for the Nusselt number was obtained using symbolic regression, and the effect of the input variables on the predictions of the best model was analyzed using Accumulated Local Effects (ALE).

The complete procedure, including preprocessing, model development, validation, performance assessment, and model interpretation, is illustrated in Figure 1.

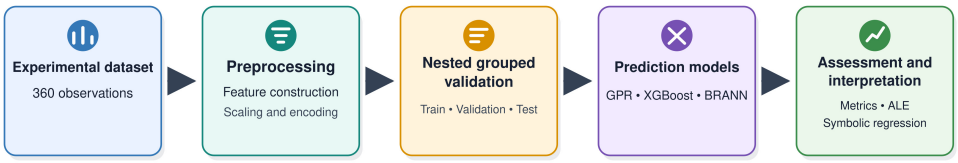


Fig. 1 Flowchart of the proposed data-driven estimation, validation, and interpretation framework.

The input and output variables considered in the two estimation tasks are summarized in Table 1.

Table 1 Input and output variables used in the estimation models

Estimation task	Input variables	Output variable
Dimensionless heat transfer estimation	Ra, θ, s/d, M	Nu
Thermal resistance estimation	$\dot{Q}_0$, θ, s/d, M	R_{th}

The two estimation relationships can be expressed as:

$$Nu = f\left(Ra, \theta, \frac{s}{d}, M\right), \tag{1}$$

$$R_{\text{th}} = g\left(\dot{Q}_0, \theta, \frac{s}{d}, M\right). \tag{2}$$

where M represents the fin material, θ is the cylinder inclination angle, s/d is the dimensionless fin spacing, and $\dot{Q}_0$ is the heating power.

2.1.1 Gaussian Process Regression

Gaussian Process Regression was employed as the principal estimation method. GPR defines a probability distribution over possible regression functions and represents the measured response as:

$$y = f(\mathbf{x}) + \varepsilon, \qquad f(\mathbf{x}) \sim \mathcal{GP}\left[m(\mathbf{x}), k(\mathbf{x}, \mathbf{x}')\right]. \tag{3}$$

where $\mathbf{x}$ is the input vector, $m(\mathbf{x})$ is the mean function, $k(\mathbf{x}, \mathbf{x}')$ is the covariance function, and ε represents normally distributed observation noise.

An automatic relevance determination form of the Matérn kernel was used so that an independent length scale could be assigned to each input variable. The kernel length scales, signal variance, and noise variance were determined by maximizing the log marginal likelihood. The optimization was repeated from 10 different initial points, with a maximum of 1000 iterations for each run, to reduce sensitivity to the initial parameter values.

In addition to the posterior mean prediction, GPR provides a predictive standard deviation for each observation. This property was used to quantify the uncertainty associated with predictions made under unseen operating and geometric conditions. For each out-of-fold observation, the lower and upper bounds of the 95% prediction interval were calculated as:

$$L_i = \hat{y}_i - 1.96\sigma_i \tag{4}$$

$$U_i = \hat{y}_i + 1.96\sigma_i \tag{5}$$

where $\hat{y}_i$ is the posterior predictive mean and σ_i is the predictive standard deviation, including the estimated observation-noise contribution. When target standardization was applied, the posterior means and interval bounds were transformed back to their original physical scales before evaluation. All prediction intervals were obtained exclusively from outer-fold test predictions. Thus, no observation used to calculate the interval-based performance measures had previously been encountered during model training or hyperparameter selection.

2.2 Extreme Gradient Boosting

XGBoost represents the estimated response as the sum of a sequence of regression trees:

$$\hat{y}_i = \sum_{k=1}^{K} f_k(\mathbf{x}_i) \tag{6}$$

where K is the number of trees and f_k denotes the contribution of the k-th regression tree. At each boosting step, a new tree is added to reduce the residual error of the preceding ensemble. Model complexity is controlled using shrinkage, subsampling, and regularization.

The maximum number of boosting rounds was set to 2000. Training was terminated when the validation error did not improve for 50 consecutive boosting rounds. The learning rate, number of trees, maximum tree depth, minimum child weight, row-sampling ratio, feature-sampling ratio, and α and λ regularization coefficients were optimized using 50 Bayesian optimization trials. The learning rate was varied between 0.01 and 0.20, the maximum tree depth between 2 and 8, and the row- and feature-sampling ratios between 0.60 and 1.00. Hyperparameter selection was based exclusively on the inner-validation RMSE.

2.3 Bayesian-Regularized Artificial Neural Network

The BRANN model consisted of an input layer, a single hidden layer, and a linear output layer. A single hidden layer was preferred because of the limited size of the experimental dataset and to avoid unnecessary model complexity. The network output can be expressed as:

$$\hat{y} = f_2(\mathbf{W}_2 f_1(\mathbf{W}_1 \mathbf{x} + \mathbf{b}_1) + \mathbf{b}_2) \tag{7}$$

where $\mathbf{W}_1$ and $\mathbf{W}_2$ are the connection-weight matrices, $\mathbf{b}_1$ and $\mathbf{b}_2$ are the bias terms, and f_1 denotes the hidden-layer activation function. A hyperbolic tangent activation function was used in the hidden layer, whereas a linear function was employed at the output.

Bayesian regularization minimizes a weighted combination of the data-fitting error and the magnitude of the network weights:

$$F = \beta E_D + \alpha E_W \tag{8}$$

where E_D is the data-fitting error, E_W is the sum of the squared network weights, and α and β are regularization parameters estimated during training.

The number of hidden neurons was selected from 5, 10, 15, 20, 25, and 30 according to the inner-validation performance. The maximum number of training epochs was set to 1000. Each network configuration was trained using 20 independent weight initializations to reduce the influence of random initialization. The architecture producing the lowest mean validation RMSE was retained and subsequently retrained using the complete development subset.

2.4 Symbolic Regression

Symbolic regression was applied separately to the Nusselt number and thermal resistance to obtain explicit correlations suitable for direct engineering calculations. The correlations for Nu were developed as functions of the Rayleigh number, inclination angle, and dimensionless fin-spacing ratio, whereas the correlations for R_{th} used the net heat input, inclination angle, and dimensionless fin-spacing ratio. Separate expressions were derived for homogeneous aluminum and functionally graded Al–Cu fins.

Accordingly, the general correlation structures were expressed as:

$$\mathrm{Nu} = f(\mathrm{Ra}, \theta, s/d) \tag{9}$$

$$R_{\mathrm{th}} = g(Q, \theta, s/d) \tag{10}$$

where θ is expressed in degrees, s/d is the dimensionless fin-spacing ratio, Q is the net heat input in W, and R_{th} is obtained in K W^{-1}. Material type was coded as $M = 0$ for homogeneous aluminum and $M = 1$ for functionally graded Al–Cu in the prediction models. However, material coding was not required in the symbolic expressions because a separate correlation was derived for each material.

The evolutionary search was performed using 20 populations, each containing 50 candidate expressions, for a maximum of 200 iterations. The permitted operators were restricted to addition, subtraction, multiplication, protected division, and physically meaningful power functions. Candidate expressions were evaluated using the outer-fold predictions, while equation selection considered both cross-validated prediction error and expression complexity. Complexity was defined according to the total number of operators, variables, and numerical constants contained in an expression. Among equations with comparable validation errors, the expression with lower complexity was selected.

The symbolic-regression structure was selected without using the outer test observations. After the final expression form had been determined, its coefficients were re-estimated using the complete experimental dataset to provide the reported engineering correlation. The performance values presented in the Results section were calculated from the combined outer-fold predictions and not from the full-data refitting stage.

2.5 Accumulated Local Effects Analysis

ALE analysis was used as the sole model-interpretation method in this study. It evaluates the local variation in model predictions over intervals of the observed input space and is less affected by correlations among the input variables than conventional partial dependence analysis.

ALE analysis was applied separately to the best-performing models for Nu and R_{th}. The Rayleigh number was divided into 20 equal-frequency intervals because it varied continuously over a sufficiently broad range. Heating power, inclination angle, and fin-spacing ratio were evaluated directly at their experimentally observed levels, since these variables contained six, six, and five discrete levels, respectively. Fin material was treated as a categorical variable, and its effect was represented by two separate ALE estimates corresponding to homogeneous aluminum and functionally graded Al–Cu fins. The resulting ALE responses were used descriptively to examine whether the relationships learned by the model were consistent with the expected heat-transfer behavior.

2.6 Model Training and Validation Strategy

A nested grouped-validation strategy was adopted to evaluate the ability of the models to estimate thermal performance under previously unseen operating conditions.

A conventional random train–test division was not used as the primary validation method because closely related observations from the same angle, power level, or fin configuration could otherwise appear simultaneously in the training and test subsets. Such a division could lead to overly optimistic performance estimates.

Three complementary outer validation schemes were implemented:

- **Leave-one-angle-out validation:** One of the six inclination angles was reserved for testing, while the remaining five angles were used for model development. Each outer fold therefore contained 300 development observations (83.3%) and 60 independent test observations (16.7%).
- **Leave-one-power-level-out validation:** One of the six heating power levels was used as the independent test group. Each fold similarly contained 300 development observations and 60 test observations.
- **Leave-one-fin-configuration-out validation:** One of the five fin configurations was reserved for testing. Each fold contained 288 development observations (80%) and 72 independent test observations (20%).

Within every outer fold, the development subset was subjected to inner grouped validation for hyperparameter selection. For the angle- and power-based analyses, the remaining five groups were evaluated using five-fold inner validation. In each inner iteration, 240 observations were used for training and 60 observations were used for validation. For the fin-configuration analysis, four-fold inner validation was applied to the remaining four configurations, resulting in 216 training observations and 72 validation observations per iteration.

The hyperparameters were selected exclusively according to the inner-validation RMSE. After the optimal configuration had been identified, the corresponding model was retrained using the entire development subset and evaluated once on the untouched outer test group. The procedure was repeated until every angle, power level, and fin configuration had served as an independent test group. Performance measures were calculated separately for each outer validation scheme using the corresponding combined out-of-fold predictions. Predictions generated under the leave-one-angle-out, leave-one-power-level-out, and leave-one-fin-configuration-out schemes were not pooled because each scheme represents a different generalization problem. Leave-one-angle-out validation was adopted as the primary evaluation scheme because cylinder inclination constitutes a central operating variable of the present study. The other two schemes were used as complementary tests of model robustness against unseen thermal loads and fin configurations. Therefore, every prediction included in the final evaluation was generated by a model that had not previously encountered the corresponding test condition.

Continuous variables were standardized separately within each training fold for GPR and BRANN. The mean and standard deviation calculated from the training data were subsequently applied to the associated validation and test data. XGBoost was trained using the original numerical scales because tree-based models do not require feature standardization. All stochastic operations, including neural-network initialization and hyperparameter optimization, were performed using a fixed random seed of 42.

The principal training and optimization settings are summarized in Table 2.

Table 2 Main training and optimization settings of the estimation methods

Method	**Main settings**
GPR	ARD Matérn kernel; 10 optimization restarts; maximum 1000 iterations; posterior mean and 95% prediction interval
XGBoost	Maximum 2000 boosting rounds; early stopping after 50 rounds; 50 Bayesian optimization trials
BRANN	One hidden layer; 5–30 hidden neurons; maximum 1000 epochs; 20 independent initializations
Symbolic regression	20 populations; 50 expressions per population; maximum 200 iterations
ALE	20 equal-frequency intervals
Hyperparameter-selection criterion	Minimum inner-validation RMSE
Final evaluation	Combined outer-fold test predictions; point-estimation and interval-based metrics
Random seed	42

Model performance was evaluated using the coefficient of determination (R^2), root mean square error (RMSE), mean absolute error (MAE), and mean absolute percentage error (MAPE):

$$R^2 = 1 - \frac{\sum_{i=1}^{N}(y_i - \hat{y}_i)^2}{\sum_{i=1}^{N}(y_i - \bar{y})^2} \tag{11}$$

$$\mathrm{RMSE} = \sqrt{\frac{1}{N}\sum_{i=1}^{N}(y_i - \hat{y}_i)^2} \tag{12}$$

$$\mathrm{MAE} = \frac{1}{N}\sum_{i=1}^{N}|y_i - \hat{y}_i| \tag{13}$$

and

$$\mathrm{MAPE} = \frac{100\%}{N}\sum_{i=1}^{N}\left|\frac{y_i - \hat{y}_i}{y_i}\right| \tag{14}$$

The calibration and sharpness of the GPR prediction intervals were evaluated using the prediction interval coverage probability (PICP), mean prediction interval width (MPIW), and normalized mean prediction interval width (NMPIW):

$$\mathrm{PICP} = \frac{1}{N}\sum_{i=1}^{N} c_i \tag{15}$$

$$\mathrm{MPIW} = \frac{1}{N}\sum_{i=1}^{N}(U_i - L_i) \tag{16}$$

$$\mathrm{NMPIW} = \frac{\mathrm{MPIW}}{y_{\max} - y_{\min}} \tag{17}$$

Here, y_i, $\hat{y}_i$, and $\bar{y}$ denote the experimental value, predicted value, and mean experimental value, respectively, while N is the number of test observations. L_i and U_i denote the lower and upper bounds of the 95% prediction interval, and c_i is an indicator function that takes a value of one when the experimental observation lies within the corresponding interval and zero otherwise. The term $y_{\max} - y_{\min}$ represents the observed range of the corresponding response in the combined outer-fold dataset. PICP measures the percentage of experimental observations enclosed by the prediction intervals. A value close to the nominal level of 95% indicates satisfactory calibration. MPIW represents the average prediction interval width, whereas NMPIW expresses this width relative to the observed response range and therefore allows the uncertainty levels of Nu and R_{th} to be compared despite their different numerical scales. All point-estimation and interval-based performance measures were calculated exclusively from the combined outer-fold test predictions. Results obtained from the different grouped-validation strategies were evaluated separately and were not pooled.

3 Results and Discussion

The performance of Gaussian process regression (GPR), Bayesian regularized artificial neural network (BRANN) and extreme gradient boosting (XGBoost) in estimating the Nusselt number and the thermal resistance of homogeneous aluminum and functionally graded Al–Cu finned cylinders is investigated in this section. Model performance was assessed based on the coefficient of determination (R^2), root mean square error (RMSE), mean absolute error (MAE) and mean absolute percentage error (MAPE). In addition to overall predictive accuracy, residual distributions were examined to determine if the residuals were centered on zero and whether the models systematically over- or under-predicted. The best performing model was then interpreted using accumulated local effects (ALE) and simplified correlations were obtained by symbolic regression.

3.1 Estimation of the Nusselt number

Figure 2 compares the experimental and estimated Nusselt numbers for both fin materials. The parity plots in Figures 2(a) and 2(b) provide an overall assessment of the three models, whereas Figures 2(c) and 2(d) show how closely the best-performing model follows the individual experimental observations for different fin configurations.

The corresponding performance indicators are presented in Table 3. GPR provided the highest predictive accuracy for both materials. For the aluminum fins, it achieved an R^2 of 0.992, with RMSE and MAE values of 0.1718 and 0.1382, respectively. A similarly strong result was obtained for the functionally graded fins, for which R^2 remained at 0.989 and MAPE was limited to 1.458%. These results indicate that GPR

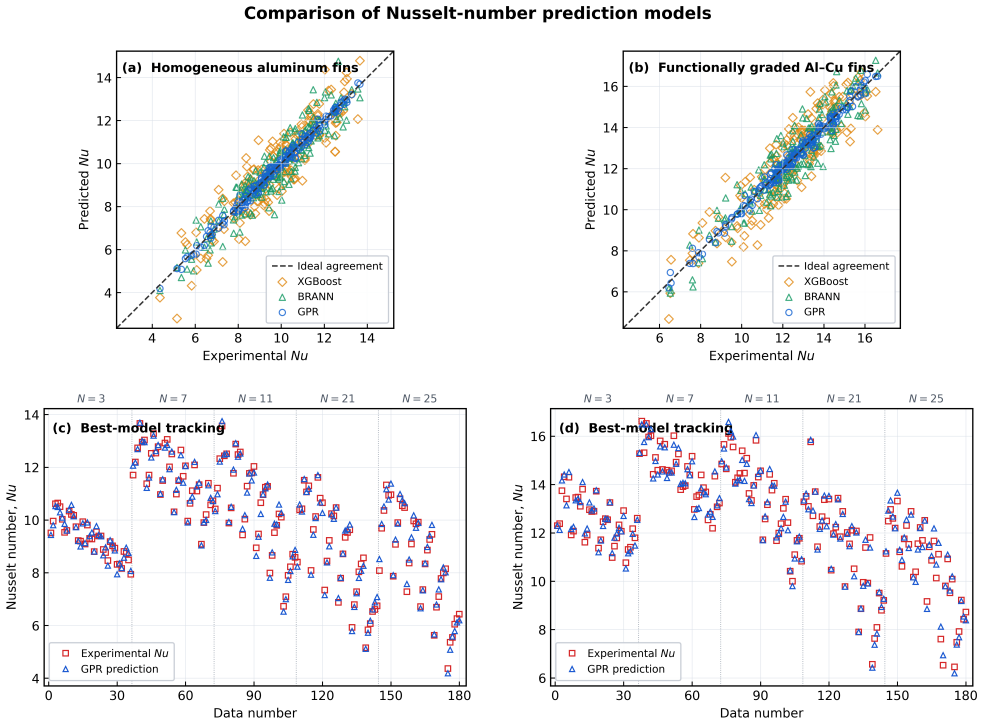


Fig. 2 Comparison of experimental and estimated Nusselt numbers based on the combined out-of-fold predictions obtained from leave-one-angle-out validation: parity plots for (a) homogeneous aluminum fins and (b) functionally graded Al–Cu fins; experimental-data tracking of the best-performing GPR model for (c) homogeneous aluminum and (d) functionally graded Al–Cu fins.

reproduced almost all of the observed variation in Nu, including the changes caused by fin number, inclination angle, heat input, and material type.

Table 3 Performance of the models in estimating the Nusselt number under leave-one-angle-out validation

Fin material	**Model**	R^2	**RMSE**	**MAE**	**MAPE (%)**
Homogeneous aluminum	GPR	0.992	0.1718	0.1382	1.518
Homogeneous aluminum	BRANN	0.865	0.7058	0.5648	6.020
Homogeneous aluminum	XGBoost	0.790	0.8803	0.7223	7.930
Functionally graded Al–Cu	GPR	0.989	0.2210	0.1751	1.458
Functionally graded Al–Cu	BRANN	0.850	0.8162	0.6724	5.564
Functionally graded Al–Cu	XGBoost	0.775	0.9996	0.8420	7.043

As seen in Figures 2(a) and 2(b), the GPR estimates remained closely distributed around the ideal agreement line over the full Nu range. BRANN followed the general trend but exhibited greater dispersion, particularly in the middle and upper

ranges. XGBoost produced the widest scatter and occasionally underestimated or overestimated the experimental values more markedly.

The tracking plots in Figures 2(c) and 2(d) provide further evidence of the response captured by GPR. The estimates closely followed both gradual changes and local variations between consecutive operating conditions. The model maintained this behavior across all five fin configurations, corresponding to N_f = 3, 7, 11, 21, and 25. The slightly higher RMSE obtained for the functionally graded fins can be associated with their wider Nu range rather than with a clear deterioration in relative prediction accuracy, as the MAPE values were comparable for the two materials.

The superior performance of GPR is reasonable for the present dataset. The thermal responses varied smoothly within a relatively low-dimensional input domain, while the available number of observations was moderate. Under these conditions, the covariance-based structure of GPR can represent nonlinear variations efficiently without requiring a very large training dataset. By comparison, BRANN and XGBoost generally benefit from a larger number of independent observations when several operating variables interact.

3.2 Estimation of thermal resistance

The estimation results for thermal resistance are presented in Figure 3. Similar to the Nusselt analysis, Figures 3(a) and 3(b) compare all three models, while Figures 3(c) and 3(d) illustrate the point-by-point tracking performance of GPR.

The numerical performance measures are reported in Table 4. GPR again provided the closest agreement with the experimental data. Its R^2 values were 0.991 and 0.988 for the homogeneous aluminum and functionally graded fins, respectively. The corresponding RMSE values remained below 0.03 K W^{-1}. BRANN ranked second, whereas XGBoost produced the largest errors for both materials.

Table 4 Performance of the models in estimating thermal resistance under leave-one-angle-out validation.

Fin material	**Model**	R^2	**RMSE (K W^{-1})**	**MAE (K W^{-1})**	**MAPE (%)**
Homogeneous aluminum	GPR	0.991	0.0275	0.0215	3.273
Homogeneous aluminum	BRANN	0.870	0.1045	0.0828	13.001
Homogeneous aluminum	XGBoost	0.800	0.1296	0.1020	15.479
Functionally graded Al–Cu	GPR	0.988	0.0298	0.0243	4.375
Functionally graded Al–Cu	BRANN	0.850	0.1052	0.0838	15.406
Functionally graded Al–Cu	XGBoost	0.780	0.1274	0.1037	18.417

The differences between the models are particularly evident at higher thermal-resistance values. In Figures 3(a) and 3(b), the GPR estimates remain close to the ideal agreement line, while the BRANN and XGBoost predictions become increasingly dispersed. The larger percentage errors obtained for R_{th} than for Nu should be interpreted in relation to the magnitude of the target variable. Because R_{th} contains

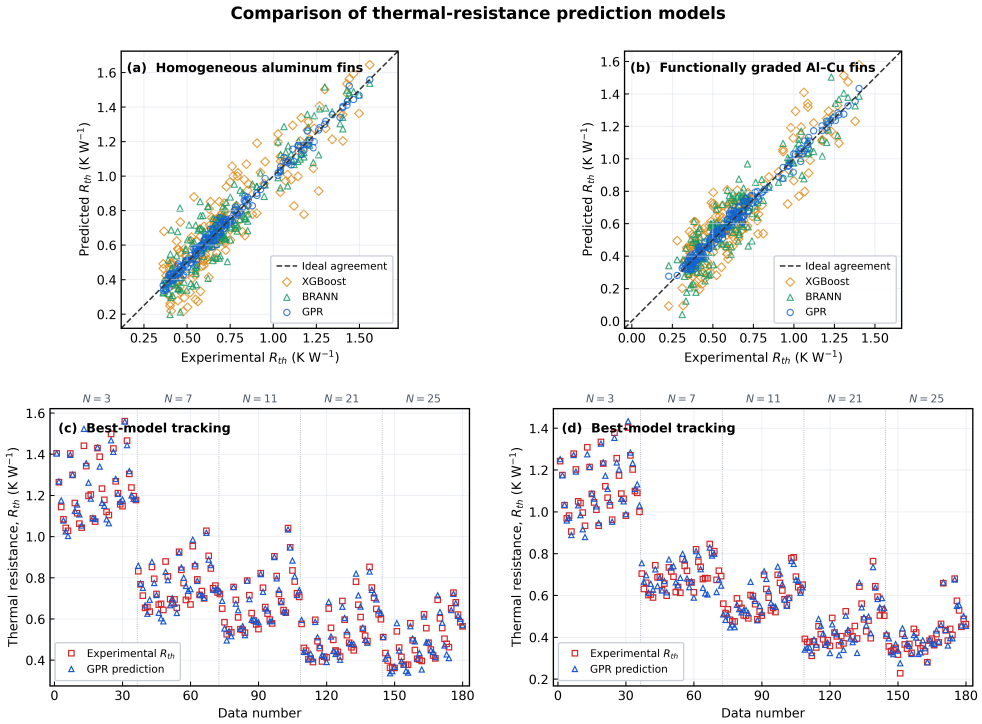


Fig. 3 Comparison of experimental and estimated thermal resistance values based on the combined out-of-fold predictions obtained from leave-one-angle-out validation: parity plots for (a) homogeneous aluminum fins and (b) functionally graded Al–Cu fins; experimental-data tracking of the best-performing GPR model for (c) homogeneous aluminum and (d) functionally graded Al–Cu fins.

relatively small values, even moderate absolute deviations can produce noticeable percentage errors. Nevertheless, GPR maintained low RMSE and MAE values for both materials.

Figures 3(c) and 3(d) show that the experimental R_{th} values decreased considerably as the fin arrangement became denser. This reduction was successfully tracked by GPR across the five fin-number groups. The model also captured the local variations within each group, which mainly resulted from changes in heat input and cylinder inclination. No pronounced deterioration was observed when the material changed from homogeneous aluminum to functionally graded Al–Cu. This suggests that the material descriptor included among the inputs allowed the model to distinguish the thermal response of the two fin structures.

Although the GPR results indicate strong surrogate-model capability, the model should be used within the investigated experimental domain. The present findings do not establish reliable extrapolation beyond heat inputs of 25–150 W, inclination angles of 0–75°, or the examined fin-spacing ratios.

3.3 Generalization to Unseen Operating and Geometric Conditions

The results presented in Figures 2 and 3 were obtained using leave-one-angle-out validation, which was selected as the primary evaluation scheme because cylinder inclination represents a central operating parameter of the investigated system. However, satisfactory performance for an unseen inclination does not necessarily ensure comparable accuracy when an entire heat-input level or fin configuration is excluded from model development. The generalization capability of GPR was therefore examined using two additional grouped-validation schemes. The resulting performance indicators are presented in Table 5.

Table 5 Generalization performance of GPR under different grouped-validation schemes.

Target	Fin material	Validation scheme	R^2	RMSE	MAE	MAI
Nu	Homogeneous aluminum	Leave-one-angle-out	0.992	0.1718	0.1382	1
Nu	Homogeneous aluminum	Leave-one-power-level-out	0.994	0.1486	0.1179	1
Nu	Homogeneous aluminum	Leave-one-fin-configuration-out	0.965	0.3587	0.2864	3
Nu	Functionally graded Al–Cu	Leave-one-angle-out	0.989	0.2210	0.1751	1
Nu	Functionally graded Al–Cu	Leave-one-power-level-out	0.992	0.1884	0.1482	1
Nu	Functionally graded Al–Cu	Leave-one-fin-configuration-out	0.958	0.4326	0.3448	2
R_{th}	Homogeneous aluminum	Leave-one-angle-out	0.991	0.0275	0.0215	3
R_{th}	Homogeneous aluminum	Leave-one-power-level-out	0.993	0.0241	0.0187	2
R_{th}	Homogeneous aluminum	Leave-one-fin-configuration-out	0.962	0.0564	0.0447	6
R_{th}	Functionally graded Al–Cu	Leave-one-angle-out	0.988	0.0298	0.0243	4
R_{th}	Functionally graded Al–Cu	Leave-one-power-level-out	0.991	0.0257	0.0206	3
R_{th}	Functionally graded Al–Cu	Leave-one-fin-configuration-out	0.954	0.0581	0.0469	8

GPR maintained strong predictive performance under all three validation schemes. For the Nusselt number, R^2 remained between 0.958 and 0.994, while MAPE varied from 1.236% to 3.121%. Thermal-resistance estimation produced R^2 values between 0.954 and 0.993, with MAPE ranging from 2.844% to 8.126%. The consistency of these results indicates that the performance of GPR was not restricted to reproducing conditions already represented in the training data.

Leave-one-power-level-out validation produced the lowest errors for both target variables. This behavior can be associated with the comparatively smooth and monotonic influence of heat input on the thermal response. Once the relationships among heat input, temperature rise, and natural convection had been learned from the remaining power levels, GPR successfully estimated the response at the excluded level.

Leave-one-fin-configuration-out validation was the most demanding scheme. Its errors were approximately twice those obtained from the primary angle-based validation, although the corresponding R^2 values remained above 0.95. Unlike heat input, the influence of fin spacing was distinctly nonlinear. In particular, the maximum convective contribution occurred at an intermediate spacing ratio rather than at either boundary of the investigated range. Estimating an entirely unseen fin configuration

therefore required the model to reconstruct a nonlinear geometric response without observing that spacing level during training.

The performance differences between the two materials remained limited. Under leave-one-fin-configuration-out validation, the MAPE values for Nu were 3.121% and 2.897% for homogeneous aluminum and functionally graded Al–Cu fins, respectively. The corresponding values for R_{th} were 6.812% and 8.126%. Thus, the inclusion of material type allowed GPR to distinguish the two thermal responses without a substantial loss of generalization capability.

Consistent with the primary validation results reported in Tables 3 and 5, GPR retained the highest accuracy under the complementary validation schemes, followed by BRANN and XGBoost. Nevertheless, these results apply only to grouped prediction within the investigated experimental domain and do not establish unrestricted extrapolation beyond the tested ranges.

3.4 Predictive Uncertainty and Interval Calibration

The predictive uncertainty of GPR was examined to determine whether its high point-estimation accuracy was accompanied by adequately calibrated prediction intervals. Unlike BRANN and XGBoost, GPR provides a posterior predictive distribution for each test observation. This distribution makes it possible to evaluate not only the expected response but also the uncertainty associated with that estimate. Figure 4 presents the out-of-fold posterior means and 95% prediction intervals obtained under the primary leave-one-angle-out validation.

As shown in Figure 4, most experimental observations were enclosed by their corresponding prediction intervals, while the posterior mean estimates remained close to the perfect-agreement line. The observations falling outside the intervals were distributed on both sides of the reference line and did not indicate a persistent tendency toward overprediction or underprediction. The intervals remained relatively narrow throughout the central response region but became wider near sparsely represented parts of the experimental domain. This behavior indicates that the uncertainty estimated by GPR responded to the amount of information available in the training data rather than remaining artificially constant over the entire prediction range.

Table 6 Calibration and sharpness of the 95% GPR prediction intervals under the grouped-validation strategies

Output	Fin material	Validation strategy	PICP (%)	MPIW	NMPIW (%)
Nu	Homogeneous aluminum	Leave-one-power-level-out	95.6	0.548	5.894
Nu	Homogeneous aluminum	Leave-one-angle-out	95.0	0.628	6.750
Nu	Homogeneous aluminum	Leave-one-fin-configuration-out	93.3	1.132	12.176
Nu	Functionally graded Al–Cu	Leave-one-power-level-out	95.0	0.666	6.555
Nu	Functionally graded Al–Cu	Leave-one-angle-out	94.4	0.793	7.810
Nu	Functionally graded Al–Cu	Leave-one-fin-configuration-out	92.8	1.396	13.740
R_{th}	Homogeneous aluminum	Leave-one-power-level-out	95.6	0.086	5.860
R_{th}	Homogeneous aluminum	Leave-one-angle-out	95.0	0.103	7.048
R_{th}	Homogeneous aluminum	Leave-one-fin-configuration-out	93.3	0.204	13.902
R_{th}	Functionally graded Al–Cu	Leave-one-power-level-out	95.0	0.091	8.166
R_{th}	Functionally graded Al–Cu	Leave-one-angle-out	94.4	0.112	10.053
R_{th}	Functionally graded Al–Cu	Leave-one-fin-configuration-out	92.8	0.221	19.833

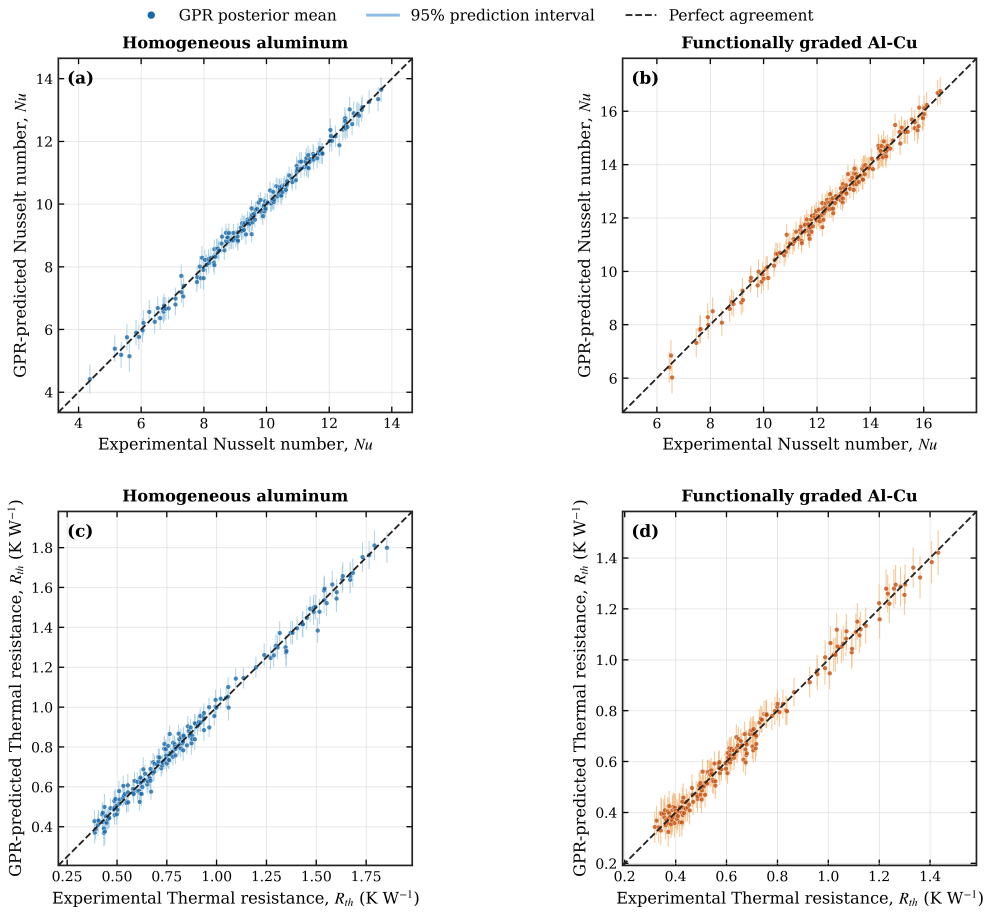


Fig. 4 Experimental values versus out-of-fold GPR predictions with 95% prediction intervals under leave-one-angle-out validation: (a) Nusselt number for homogeneous aluminum fins, (b) Nusselt number for functionally graded Al–Cu fins, (c) thermal resistance for homogeneous aluminum fins, and (d) thermal resistance for functionally graded Al–Cu fins.

The interval-based performance measures obtained under the three grouped-validation strategies are summarized in Table 6. Under leave-one-angle-out validation, PICP values ranged from 94.4% to 95.0%, while NMPIW varied between 6.750% and 10.053%. Leave-one-power-level-out validation produced the sharpest intervals, with PICP values of 95.0–95.6% and NMPIW values of 5.860–8.166%.

Leaving out an entire fin configuration produced the widest intervals. In this case, PICP decreased slightly to 92.8–93.3%, while NMPIW increased to 12.176–13.740% for Nu and 13.902–19.833% for R_{th}. This result is consistent with the point-estimation analysis and confirms that predicting an unseen geometric arrangement was more demanding than estimating an excluded power level.

3.5 Residual characteristics of the prediction models

Performance metrics provide an overall measure of accuracy but do not fully reveal the structure of the prediction errors. Figure 5 therefore presents the residual distributions for each target variable and fin material. The residual was defined as the difference between the predicted and experimental values. Consequently, a positive residual indicates overprediction, whereas a negative residual represents underprediction.

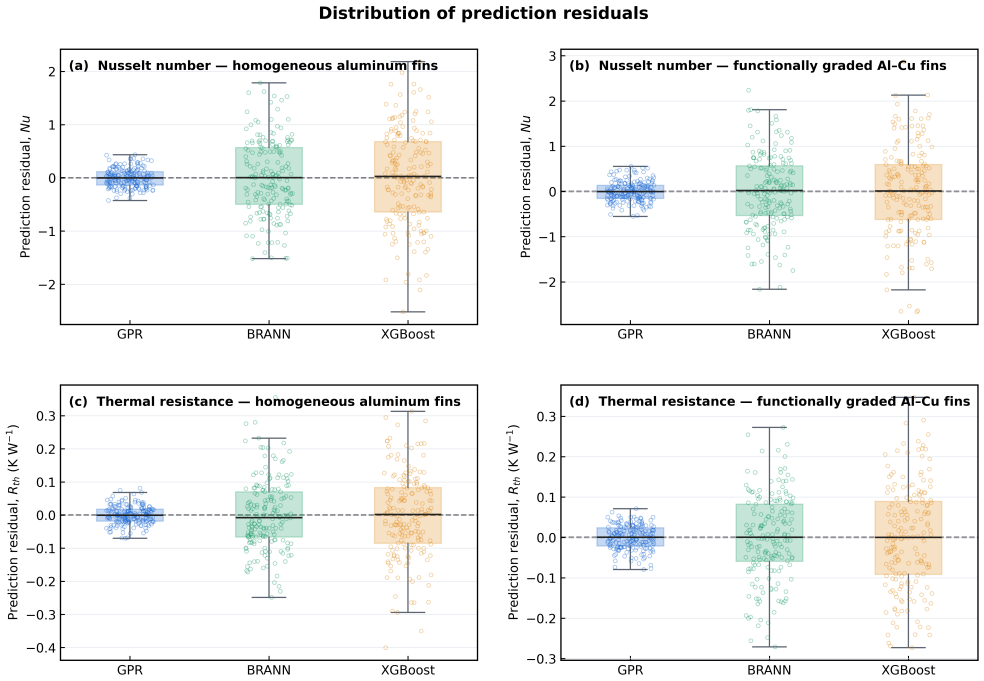


Fig. 5 Residual distributions of GPR, BRANN, and XGBoost for (a) Nusselt number of homogeneous aluminum fins, (b) Nusselt number of functionally graded Al–Cu fins, (c) thermal resistance of homogeneous aluminum fins, and (d) thermal resistance of functionally graded Al–Cu fins.

For all four cases, the median GPR residual remained close to zero, and its interquartile range was noticeably smaller than those of BRANN and XGBoost. This result is consistent with the RMSE and MAE values reported in Tables 3 and 4. More importantly, the GPR residuals were distributed on both sides of zero. The absence of a pronounced shift in their median indicates that the model did not consistently overestimate or underestimate either Nu or R_{th}.

BRANN also produced residuals centered approximately around zero, but their dispersion was considerably larger. XGBoost showed the broadest distributions and the most pronounced extreme errors, particularly for the Nusselt number of functionally graded fins. A similar pattern was observed for thermal resistance, although the residual magnitudes were smaller because of the scale of R_{th}. These findings confirm

that the ranking of the models was not determined by a small number of isolated observations; it remained visible throughout the overall error distributions.

The wider BRANN and XGBoost residuals should not necessarily be interpreted as a general limitation of these techniques. Instead, they indicate that their present configurations were less suitable for the size and structure of this dataset. The combination of a limited experimental sample, several discrete operating conditions, and smooth physical relationships favored GPR.

3.6 Physical interpretation of the GPR model

Since GPR produced the lowest prediction errors for both target variables, ALE analysis was applied to this model. ALE was preferred because it estimates the average local contribution of each input while reducing the distortion that may occur when the explanatory variables are correlated. The effects are centered around zero; therefore, positive ALE values increase the estimated response relative to its average, whereas negative values decrease it.

3.6.1 Effects of the input variables on the Nusselt number

Figure 6 presents the effects of the Rayleigh number, inclination angle, fin-spacing ratio, and fin material on the GPR estimates of Nu.

As shown in Figure 6(a), the Rayleigh number had a positive and monotonic effect on Nu. The ALE contribution increased from approximately -2.3 at the lowest Ra level to above $+3.0$ at the upper end of the investigated range. This behavior agrees with the expected strengthening of buoyancy-driven flow as the temperature difference and Rayleigh number increase.

Inclination angle had the opposite effect. Figure 6(b) indicates a progressive reduction in Nu as the cylinder was rotated from 0° to 75°. The effect remained positive up to approximately 45°, after which it became distinctly negative. The sharp reduction at 60° and 75° suggests that the orientation increasingly restricted the development and removal of the heated air plume from the fin passages.

The fin-spacing response in Figure 6(c) was nonlinear. The largest positive contribution was obtained at $s/d = 1.480$, corresponding to the seven-fin configuration. This indicates that the highest normalized convective performance did not occur at either the widest or narrowest spacing. Widely spaced fins provide insufficient surface augmentation, whereas excessively narrow passages may restrict natural circulation and promote interaction between adjacent thermal boundary layers. The intermediate spacing therefore provided a more favorable balance between added surface area and airflow accessibility.

The material effect in Figure 6(d) shows that functionally graded Al–Cu fins increased the estimated Nu relative to homogeneous aluminum fins. This finding indicates that the material distribution influenced the surface-temperature field and, consequently, the convective response represented by the Nusselt number.

3.6.2 Effects of the input variables on thermal resistance

The ALE results obtained for thermal resistance are shown in Figure 7.

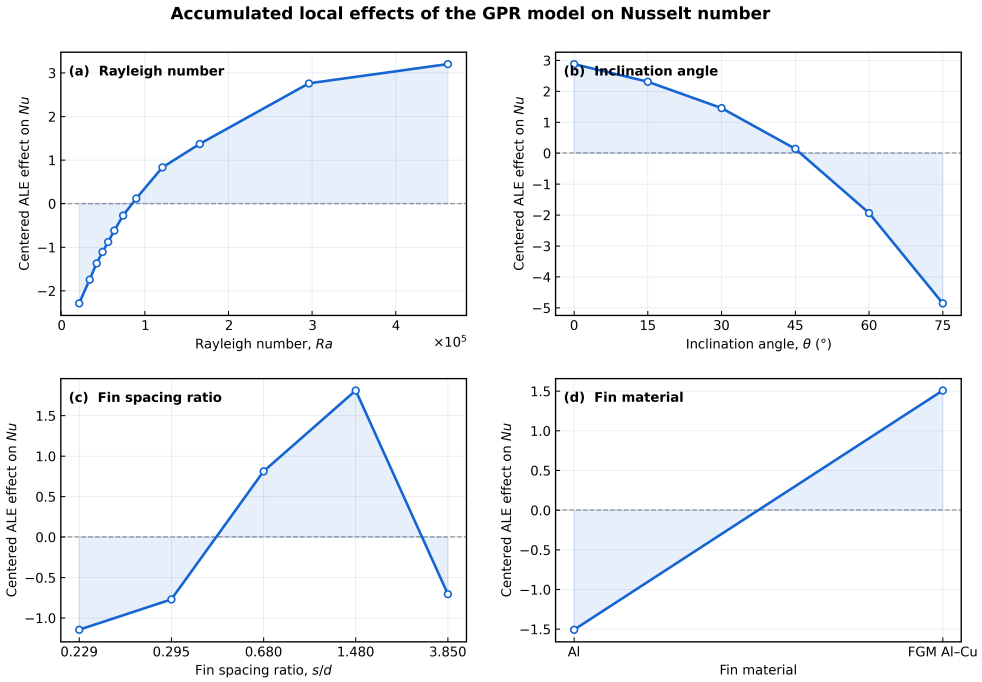


Fig. 6 Accumulated local effects of the GPR input variables on the estimated Nusselt number: (a) Rayleigh number, (b) inclination angle, (c) fin-spacing ratio, and (d) fin material.

Figure 7(a) demonstrates that increasing heat input reduced the centered contribution to R_{th}. The effect decreased from approximately $+0.125$ K W^{-1} at 25 W to about -0.080 K W^{-1} at 150 W. This trend reflects the enhancement of natural convection at higher heat inputs, which limits the rise in surface temperature relative to the supplied heat rate.

The inclination effect shown in Figure 7(b) supports the interpretation of the Nu results. Thermal resistance increased with inclination angle, becoming positive above approximately 45° and reaching its highest level at 75°. Thus, the orientations associated with weaker convective transport produced a simultaneous reduction in Nu and increase in R_{th}.

Figure 7(c) shows that smaller fin-spacing ratios reduced thermal resistance. The largest positive contribution occurred at $s/d = 3.850$, corresponding to the lowest fin number. This result does not conflict with the maximum Nu contribution observed at $s/d = 1.480$. The Nusselt number characterizes normalized convective behavior, whereas thermal resistance reflects the combined influence of heat-transfer area, conduction, and temperature rise. Consequently, a dense fin arrangement may reduce overall thermal resistance through increased surface area even when it does not maximize the normalized convection coefficient.

Finally, Figure 7(d) indicates that functionally graded Al–Cu fins decreased thermal resistance compared with homogeneous aluminum fins. This negative contribution,

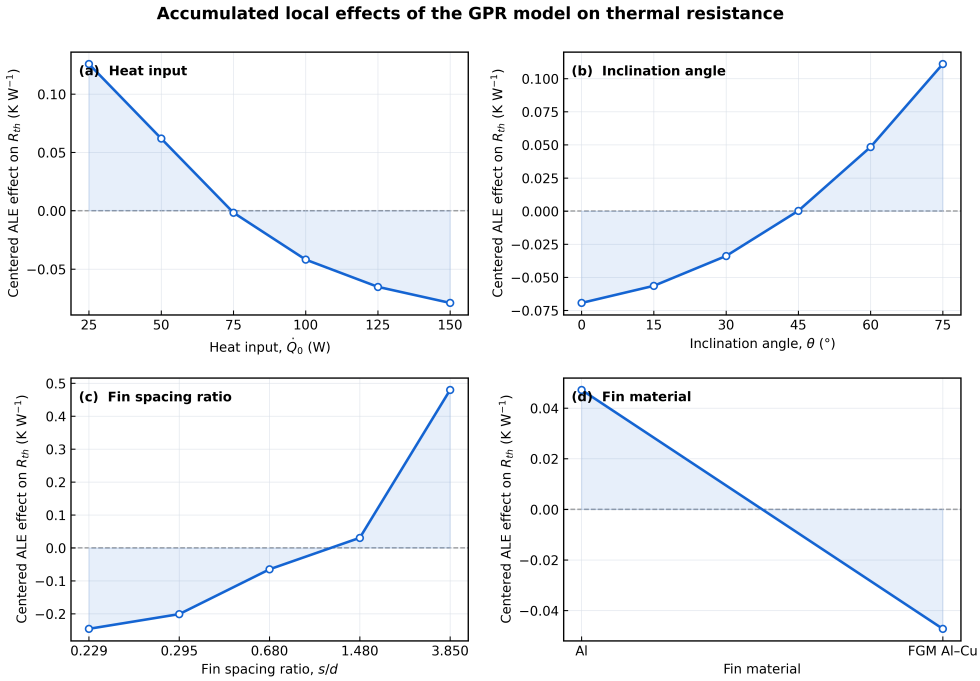


Fig. 7 Accumulated local effects of the GPR input variables on the estimated thermal resistance: (a) heat input, (b) inclination angle, (c) fin-spacing ratio, and (d) fin material.

together with the positive material contribution to Nu in Figure 6(d), confirms that the functionally graded configuration produced a favorable thermal response within the investigated operating range.

3.7 Symbolic-regression correlations

Although GPR provided the highest predictive accuracy, its covariance-based structure does not yield a compact analytical expression that can be applied directly without the trained model. Symbolic regression was therefore used to derive separate correlations for Nu and R_{th}. Different expressions were obtained for homogeneous aluminum and functionally graded Al–Cu fins to account for their distinct thermal responses. The final correlation structures were selected by considering both outer-fold prediction performance and expression complexity.

To improve numerical conditioning and retain compact coefficient values, the variables used in the symbolic expressions were normalized according to:

$$X = \ln\left(\frac{Ra}{10^5}\right) \tag{18}$$

$$W = \ln\left(\frac{Q_0}{Q_{\text{ref}}}\right), \quad Q_{\text{ref}} = 100 \text{ W} \tag{19}$$

$$Y = \frac{\theta}{75^\circ} \tag{20}$$

$$Z = \ln\left(\frac{s}{0.68}\right) \tag{21}$$

Following the selection of the symbolic structures, the coefficients were re-estimated using the complete experimental dataset. The resulting material-specific engineering correlations are given as follows:

$$\begin{aligned} Nu_{\text{Al}} =& 14.3879 + 1.8706X - 0.4354X^2 - 0.9850Y - 6.8032Y^2 \\ &+ 0.1837Z - 1.1695Z^2 + 0.3737XY + 0.0469XZ + 1.3973YZ \end{aligned} \tag{22}$$

$$\begin{aligned} Nu_{\text{FGM}} =& 16.2438 + 0.5945X - 0.2683X^2 + 0.2943Y - 6.4307Y^2 \\ &+ 1.1919Z - 1.3984Z^2 + 1.0784XY + 0.3497XZ + 0.5419YZ \end{aligned} \tag{23}$$

$$\begin{aligned} R_{\text{th,Al}} =& 0.5506 - 0.1076W + 0.0152W^2 - 0.0055Y + 0.2494Y^2 \\ &+ 0.2468Z + 0.1181Z^2 - 0.0691WY - 0.0144WZ - 0.0344YZ \end{aligned} \tag{24}$$

$$\begin{aligned} R_{\text{th,FGM}} =& 0.4652 - 0.0673W - 0.0023W^2 + 0.0248Y + 0.1295Y^2 \\ &+ 0.1915Z + 0.0815Z^2 - 0.0681WY - 0.0377WZ - 0.0306YZ \end{aligned} \tag{25}$$

In these expressions, Nu and R_{th} are dimensionless, Q is the net heat input expressed in W, θ is the inclination angle expressed in degrees, and the fin-spacing ratio is dimensionless. The calculated value of R_{th} is obtained in K/W. Because separate equations were derived for the two materials, an additional material-coding parameter is not required in the symbolic correlations.

The correlations are restricted to the experimental domain used in their development: Ra range, inclination angles, and approximately the investigated fin-spacing ratio. The applicable net heat-input ranges are 20.89–140.38 W for the aluminum fins and 23.90–146.82 W for the functionally graded Al–Cu fins. Extrapolation beyond these ranges, particularly to an inclination angle of 90°, is not recommended without additional experimental validation.

The coefficients presented in Equations 22–25 correspond to the final correlations refitted using the complete dataset. By contrast, the predictions presented in Figure 8 and the performance measures reported in Table 7 were obtained by combining the outer-fold predictions. Therefore, the reported statistical performance reflects predictions for observations that were not used when estimating the corresponding fold-specific coefficients.

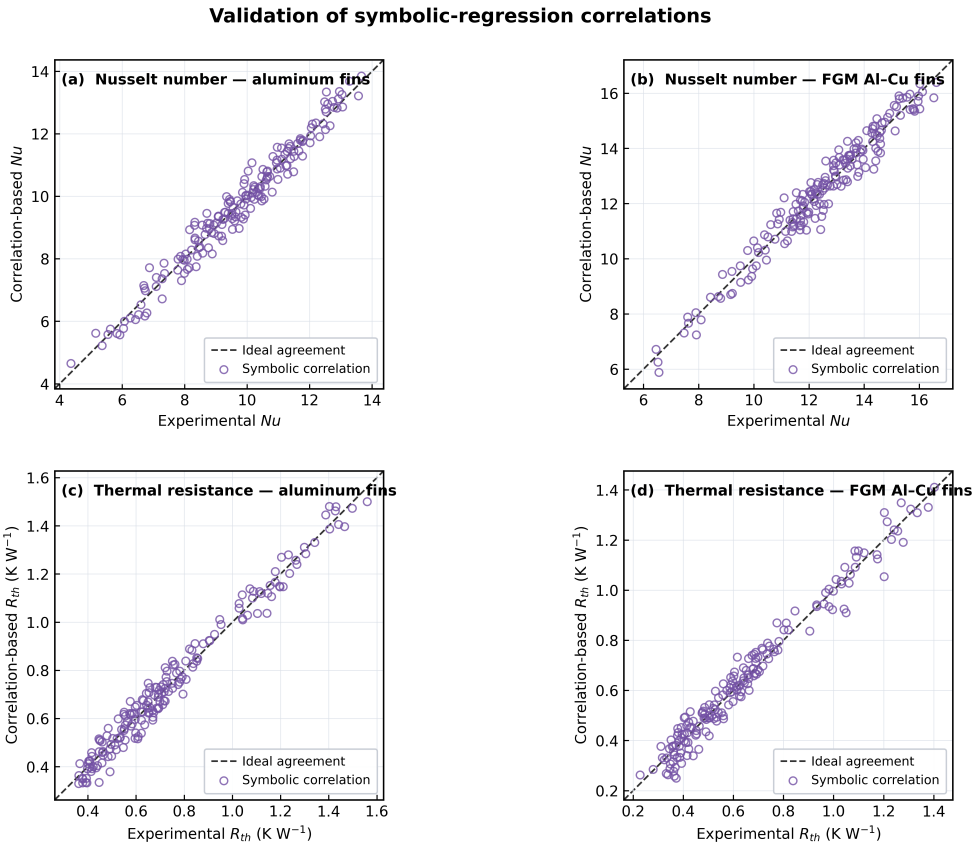


Fig. 8 Comparison of the outer-fold symbolic-regression predictions with the experimental measurements: Nusselt number for (a) homogeneous aluminum and (b) functionally graded Al–Cu fins; thermal resistance for (c) homogeneous aluminum and (d) functionally graded Al–Cu fins.

The correlation-based predictions were concentrated around the ideal agreement line for all four cases. Their statistical performance is summarized in Table 7. The R^2 values ranged from 0.955 to 0.975, demonstrating that the simplified expressions retained most of the relationships captured by the experimental dataset.

The correlation-based predictions were concentrated around the ideal agreement line for all four cases. Their statistical performance is summarized in Table 7. The Nu correlations produced MAPE values close to 3%, while the R_{th} correlations remained below 7% for both materials.

The distinction between the two modelling approaches is therefore important. GPR is preferable when maximum predictive accuracy is required and computational implementation is available. The symbolic correlations offer lower accuracy but greater transparency and ease of use. They should be regarded as complementary engineering tools rather than replacements for the more accurate GPR model.

Table 7 Statistical performance measures of the symbolic regression correlations.

Target variable	Fin material	R^2	RMSE	MAE	MAPE (%)
Nu	Homogeneous aluminum	0.965	0.3594	0.2896	3.146
Nu	Functionally graded Al–Cu	0.955	0.4470	0.3698	3.056
R_{th}	Homogeneous aluminum	0.975	0.0458 $\mathrm{K\,W^{-1}}$	0.0379 $\mathrm{K\,W^{-1}}$	5.777
R_{th}	Functionally graded Al–Cu	0.968	0.0486 $\mathrm{K\,W^{-1}}$	0.0382 $\mathrm{K\,W^{-1}}$	6.908

Overall, GPR provided the most accurate representation of both thermal responses, whereas the symbolic-regression correlations offered a simpler and more transparent alternative for engineering calculations. These models should nevertheless be used within the investigated ranges of heat input, inclination angle, fin-spacing ratio, and material type. Predictions for a 90° inclination or operating and geometric conditions outside the experimental domain require additional validation.

4 Conclusions

This study established a unified data-driven framework for estimating the Nusselt number and thermal resistance of inclined cylinders equipped with homogeneous aluminum and functionally graded Al–Cu annular fins. GPR, BRANN, and XGBoost were evaluated using 360 experimental observations covering different heat inputs, inclination angles, fin-spacing ratios, and material configurations. The predictive comparison was complemented by accumulated local effects analysis and symbolic regression, thereby linking model accuracy with physical interpretation and practical engineering use.

GPR provided the most accurate and consistent estimates for both thermal responses and fin materials. Under the primary leave-one-angle-out validation, its R^2 values ranged from 0.989 to 0.992 for Nu and from 0.988 to 0.991 for R_{th}. When all three grouped validation strategies were considered, GPR maintained R^2 values of 0.958–0.994 for Nu and 0.954–0.993 for R_{th}. Excluding an entire fin configuration represented the most demanding generalization case, whereas excluding a power level produced comparatively smaller accuracy losses. This distinction indicates that interpolation across the smooth thermal response to heat input is less challenging than predicting the behavior of an unseen geometric arrangement. The nearly zero-centered and narrow residual distributions further showed that the GPR estimates were not affected by a pronounced tendency toward overprediction or underprediction.

BRANN reproduced the main response trends but exhibited greater error dispersion, while XGBoost provided the lowest accuracy under the present data conditions.

The ALE analysis confirmed that the GPR responses were consistent with the expected heat-transfer behavior. Increasing the Rayleigh number enhanced Nu, whereas increasing the inclination angle weakened natural convection and increased R_{th}. The influence of fin spacing was nonlinear. An intermediate spacing ratio produced the strongest positive contribution to the normalized convective response by

providing a favorable balance between airflow accessibility and boundary-layer interaction. Denser fin arrangements, however, reduced overall thermal resistance because of their greater available heat-transfer area. The functionally graded Al–Cu fins generally produced higher Nu and lower R_{th} values than the homogeneous aluminum fins within the investigated operating range, demonstrating the thermal benefit of the graded material configuration.

The symbolic-regression correlations explained a substantial proportion of the experimental variation, with R^2 values ranged from 0.955 to 0.975. Although their predictive accuracy remained below that of GPR, these correlations offer a transparent and readily applicable alternative when an explicit analytical expression is more practical than a trained model. The main contribution of this study therefore lies not only in identifying the most accurate estimation method, but also in combining grouped generalization assessment, physically meaningful interpretation, and compact engineering correlations within a single framework.

The developed models and correlations should be applied within the investigated domain: heat inputs of 25–150 W, inclination angles of 0°–75°, and the examined fin-spacing and material configurations. Predictions for a 90° inclination or for operating and geometric conditions outside these ranges require additional experimental validation. Future work should extend the dataset to intermediate fin spacings, alternative graded-material distributions, and transient thermal conditions. Such developments would strengthen out-of-domain generalization and support the use of the proposed framework in the design and optimization of naturally cooled annular-finned systems.

References

[1] AlBaidani, M.M., Mishra, N.K., Alam, M.M., Eldin, S.M., AL-Zahrani, A.A., Akgül, A.: Numerical analysis of magneto-radiated annular fin natural-convective heat transfer performance using advanced ternary nanofluid considering shape factors with heating source. Case Studies in Thermal Engineering **44**, 102825 (2023) https://doi.org/10.1016/j.csite.2023.102825

[2] Alharbi, K.A.M., Bani-Fwaz, M.Z., Eldin, S.M., Akgül, A.: Thermal management in annular fin using ternary nanomaterials influenced by magneto-radiative phenomenon and natural convection. Scientific Reports **13**(1), 9528 (2023) https://doi.org/10.1038/s41598-023-36418-4

[3] Aich, W., Almujibah, H., Abdullaev, S., Bani-Fwaz, M.Z., Hassan, A.M.: Thermal performance of radiated annular extended surface using advanced nanomaterials influenced by various physical controlling parameters for nucleate boiling case. Case Studies in Thermal Engineering **51**, 103524 (2023) https://doi.org/10.1016/j.csite.2023.103524

[4] Bahlekeh, A., Mohammed, H.I., Al-Azzawi, W.K., Dulaimi, A., Majdi, H.S., Talebizadehsardari, P., Mahdi, J.M.: Cfd analysis on optimizing the annular fin parameters toward an improved storage response in a triple-tube containment system. Energy Science & Engineering **10**(12), 4814–4839 (2022) https://doi.org/10.1002/ese3.1310

[5] Han, Z., Ding, S., Liu, Q., Ge, W.: Optimization study of performance for latent heat thermal energy storage unit with non-uniform annular perforated fins based on response surface methodology. Applied Thermal Engineering **279**, 127510 (2025) https://doi.org/10.1016/j.applthermaleng.2025.127510

[6] Amiri, A., Karami, A., Yousefi, T., Zanjani, M.: Artificial neural network to predict the natural convection from vertical and inclined arrays of horizontal cylinders. Polish Journal of Chemical Technology **14**(4), 46–52 (2012) https://doi.org/10.2478/v10026-012-0101-6

[7] Roy, K., Das, B., Pathak, K.K., Giri, A.: Thermo-hydraulic analysis of slightly inclined finned channel under natural convection. Journal of Applied Fluid Mechanics **15**(4), 985–998 (2022) https://doi.org/10.47176/jafm.15.04.33307

[8] Jubear, A.J., Al-Waaly, A.A.Y., Saha, G.: Experimental and numerical investigation of the effect of interrupted, inclined, and staggered rectangular-fin arrays on heat sink performance. Heat Transfer **55**(1), 713–728 (2025) https://doi.org/10.1002/htj.70102

[9] Eleiwi, M.A., Tahseen, T.A., Ghareeb, A.: Intelligent control based estimation of heat transfer coefficient from four flat tubes with different attack air angles. Journal of Advanced Research in Fluid Mechanics and Thermal Sciences **72**(2),

65–78 (2020) https://doi.org/10.37934/arfmts.72.2.6578

[10] Kim, D., Kim, D.-K.: Orientation effects of curved finned cylinders under natural convection. Journal of Mechanical Science and Technology **39**(2), 983–995 (2025) https://doi.org/10.1007/s12206-025-0140-6

[11] Sulaiman, M., Khalaf, O.I., Khan, N.A., Alshammari, F.S., Algburi, S., Hamam, H.: Machine learning-based prediction of heat transfer performance in annular fins with functionally graded materials. Scientific Reports **14**(1), 8801 (2024) https://doi.org/10.1038/s41598-024-58595-6

[12] Dogmaz, M.A., Şafak, İ., Güneş, S., Reddy, J.N.: An investigation of the thermal performance of functionally graded annular fins on a horizontal cylinder under natural convection. Experimental Heat Transfer **38**(6), 729–751 (2025) https://doi.org/10.1080/08916152.2024.2396337

[13] Şafak, İ., Dogmaz, M.A., Güneş, S.: Experimental investigation of natural convection heat transfer from functionally graded annular fins on an inclined cylinder. Proceedings of the Institution of Mechanical Engineers, Part C: Journal of Mechanical Engineering Science **239**(12), 4774–4791 (2025) https://doi.org/10.1177/09544062251322392

[14] Şafak, İ., Şenyiğit, E., Güneş, S., Doğmaz, M.A.: Investigation of heat transfer in functionally graded annular fins under natural convection using taguchi methods. Journal of Thermal Analysis and Calorimetry **150**(14), 10839–10853 (2025) https://doi.org/10.1007/s10973-025-14484-2

[15] Cho, H.W., Park, Y.G., Seo, Y.M., Ha, M.Y.: Prediction of the heat transfer performance of mixed convection in a lid-driven enclosure with an elliptical cylinder using an artificial neural network. Numerical Heat Transfer, Part A: Applications **78**(2), 29–47 (2020) https://doi.org/10.1080/10407782.2020.1777793

[16] Karami, A., Yousefi, T., Harsini, I., Maleki, E., Mahmoudinezhad, S.: Neuro-fuzzy modeling of the free convection heat transfer from a wavy surface. Heat Transfer Engineering **36**(9), 847–855 (2014) https://doi.org/10.1080/01457632.2015.963444

[17] Bhran, A.A., Maghrabie, H.M., Gadallah, A.G., Fawaz, H.E.: Experimental investigation and ann-based prediction of average nusselt number for a flat surface subjected to double inclined air jets. Scientific Reports **15**(1), 37738 (2025) https://doi.org/10.1038/s41598-025-18142-3

[18] Calisir, T., Çolak, A.B., Aydin, D., Dalkilic, A.S., Baskaya, S.: Artificial neural network approach for investigating the impact of convector design parameters on the heat transfer and total weight of panel radiators. International Journal of Thermal Sciences **183**, 107845 (2023) https://doi.org/10.1016/j.ijthermalsci.2022.107845

[19] Çolak, A.B., Akgül, D., Mercan, H., Dalkilic, A.S., Wongwises, S.: Estimation of heat transfer parameters of shell and helically coiled tube heat exchangers by machine learning. Case Studies in Thermal Engineering **42**, 102713 (2023) https://doi.org/10.1016/j.csite.2023.102713

[20] Mercan, H., Sonmez, F., Çolak, A.B., Dalkilic, A.S.: Determination of heat transfer rates of heavy-duty radiators for trucks having flattened and double-u grooved pipes with louvered fins by ann method: An experimental study. The European Physical Journal Plus **137**, 382 (2022) https://doi.org/10.1140/epjp/s13360-022-02578-x

[21] Çolak, A.B., Kirkar, S.M., Gönül, A., Dalkilic, A.S.: Assessment of heat transfer characteristics of a corrugated heat exchanger based on various corrugation parameters using artificial neural network approach. International Journal of Heat and Fluid Flow **108**, 109455 (2024) https://doi.org/10.1016/j.ijheatfluidflow.2024.109455

[22] Durmuşoğlu, A., Turgut, B., Tekin, Y., Turgut, B.: Estimation of the effect of oblique positioned obstacle placement on thermal performance of a horizontal mantle hot water tank with machine learning. Applied Sciences **15**(1), 48 (2025) https://doi.org/10.3390/app15010048

[23] Çorumlu, V., Altıntaş, V., Abuşka, M.: Evaluation of prediction and modeling performance using machine learning methods for thermal parameters of heat sinks under forced convection: The case of external validation. International Communications in Heat and Mass Transfer **151**, 107228 (2024) https://doi.org/10.1016/j.icheatmasstransfer.2023.107228

[24] Afzal, A., Lee, S., Kim, S.-M., Mudawar, I.: Gaussian process regression to predict dryout incipience quality of saturated flow boiling in mini/micro-channels. Applied Thermal Engineering **256**, 124137 (2024) https://doi.org/10.1016/j.applthermaleng.2024.124137

[25] Noh, H., Lee, S., Kim, S.-M., Mudawar, I.: Utilization of xgboost algorithm to predict dryout incipience quality for saturated flow boiling in mini/micro-channels. International Journal of Heat and Mass Transfer **231**, 125827 (2024) https://doi.org/10.1016/j.icheatmasstransfer.2024.125827

[26] Biswal, G., Meshram, G.S.: Machine learning-based prediction of nusselt number for vertical helical coils in natural convection heat transfer. International Communications in Heat and Mass Transfer **164**, 108983 (2025) https://doi.org/10.1016/j.icheatmasstransfer.2025.108983